AIMS Mathematics, 6(11): 12599–12618.
DOI: 10.3934/math.2021726
Received: 05 July 2021
Accepted: 24 August 2021
Published: 01 September 2021

http://www.aimspress.com/journal/Math

Research article

Analysis of 2D heat conduction in nonlinear functionally graded materials using a local semi-analytical meshless method

Chao Wang[1], Fajie Wang[1,2,*] and Yanpeng Gong[3,*]

[1] College of Mechanical and Electrical Engineering, National Engineering Research Center for Intelligent Electrical Vehicle Power System, Qingdao University, Qingdao 266071, China
[2] Institute of Mechanics for Multifunctional Materials and Structures, Qingdao University, Qingdao 266071, China
[3] Institute of Electronics Packaging Technology and Reliability, Faculty of Materials and Manufacturing, Beijing University of Technology, Beijing 100124, China.

* **Correspondences:** Email: wfj1218@126.com, yanpeng.gong@bjut.edu.cn;
Tel: +86053285953800; Fax: +86053285953800.

Abstract: This paper proposes a local semi-analytical meshless method for simulating heat conduction in nonlinear functionally graded materials. The governing equation of heat conduction problem in nonlinear functionally graded material is first transformed to an anisotropic modified Helmholtz equation by using the Kirchhoff transformation. Then, the local knot method (LKM) is employed to approximate the solution of the transformed equation. After that, the solution of the original nonlinear equation can be obtained by the inverse Kirchhoff transformation. The LKM is a recently proposed meshless approach. As a local semi-analytical meshless approach, it uses the non-singular general solution as the basis function and has the merits of simplicity, high accuracy, and easy-to-program. Compared with the traditional boundary knot method, the present scheme avoids an ill-conditioned system of equations, and is more suitable for large-scale simulations associated with complicated structures. Three benchmark numerical examples are provided to confirm the accuracy and validity of the proposed approach.

Keywords: semi-analytical meshless method; local knot method; Kirchhoff transformation; nonlinear functionally graded material; heat conduction
Mathematics Subject Classification: 65N35, 68W99, 80M22

1. Introduction

The functionally graded material is a composite with continuously varying microstructure and mechanical properties and is often applied to reduce the thermal stress or residual stress in dissimilar material joints. With this regard, it is very important to analyze the heat transfer characteristics of functionally graded materials. Generally, it is not easy work to derive an exact expression of temperature distribution in nonlinear functionally graded materials. Therefore, the numerical simulation has become one of the main methods for addressing such problems.

Over the past few decades, various numerical methods have been developed for the analysis of heat transfer in functionally graded materials. The main methods include the finite element method (FEM) [1–4], the boundary element method (BEM) [5–7], and the finite difference method (FDM) [8–10]. Among them, the FEM occupies dominant position due to its mature theory system and good stability. These traditional mesh-type methods have their advantages, but at the same time they have many deficiencies, such as the complexity of preprocessing, especially for complex structures.

In order to reduce the time-consuming task of grid partition, numerous meshless/meshfree methods and coupled finite element-meshfree methods [11,12] have been proposed in recent years. At present, the common meshless methods include the meshless local Petrov-Galerkin method (MLPG) [13–15], the generalized finite difference method (GFDM) [16–19], the singular boundary method (SBM) [20–24], the boundary knot method (BKM) [25–28] and the method of fundamental solution (MFS) [29–32], etc. The successful application of these approaches shows their development prospect. Meanwhile, these methods also have some limitations. For example, as the semi-analytical and boundary-type meshless schemes, the BKM and MFS encounter the challenge of simulating large-scale and/or high-dimensional problems. With these reasons in mind, the localized method of fundamental solution (LMFS) [33] and the localized boundary knot method (LBKM) [34] have been proposed and successfully applied to large-scale acoustics [35,36], elastic mechanics [37], inverse problems [38], steady-state heat transfers [39,40] and other mechanics problems [41–43].

The LBKM is a domain-type meshfree approach using the non-singular general solution as the basis function. In fact, it can be regarded as a localized version of traditional boundary-type BKM. When this method was first proposed, the artificial boundaries and boundary nodes on it are required for every local subdomain. Later, the LBKM is modified into the local knot method (LKM) without designing the artificial boundaries. Like the local radial basis function collocation method and the element-free Galerkin method [44–46], the LKM is a typical localized domain-type meshless method. Unlike them, the LKM is a semi-analytical and strong-form approach, in which the nonsingular general solution is taken as the basis function. Compared with the local radial basis function collocation method, the LKM avoids the issue of selecting shape parameters, and has a higher numerical accuracy. Recently, the LKM has been successfully applied to solving convection-diffusion-reaction equations [47] and acoustic problems [48], and has demonstrated the advantages of truly meshless, high-accuracy, and large-scale calculation.

In view of its above merits, this study makes a first attempt to employ the LKM in conjunction with the Kirchhoff transformation to solve the heat conduction problems of two-dimensional non-linear functionally graded materials. In the calculation, the Kirchhoff transformation is applied to transform the nonlinear heat conduction equation into a linear equation. The transformed equation is a modified Helmholtz equation whose non-singular general solution is available. The LKM can be directly used to approximate the solution of the modified Helmholtz equation. The solution of the

original problem can be acquired by using the inverse Kirchhoff transformation.

The general outline of this paper is as follows. The heat conduction problem of functionally graded nonlinear material is introduced in Section 2. Section 3 describes the procedures of solving the anisotropic modified Helmholtz equation via the LKM. In Section 4, three benchmark numerical examples are presented to demonstrate the feasibility and accuracy of the proposed methodology. Finally, some conclusions are drawn in Section 5.

2. Problem statement

Consider the steady-state heat conduction problem in a two-dimensional nonlinear functionally graded material with the domain $\Omega \subset R^2$ and boundary Γ, the governing equation can be represented as

$$\sum_{i,j=1}^{2} \frac{\partial}{\partial x_i}(K_{ij}(\boldsymbol{x},T)\frac{\partial T(\boldsymbol{x})}{\partial x_j}) = 0, \quad \boldsymbol{x} \in \Omega, \tag{1}$$

with the following boundary conditions:

$$T(\boldsymbol{x}) = \bar{T}, \quad \boldsymbol{x} \in \Gamma_D, \tag{2}$$

$$\frac{\partial T(\boldsymbol{x})}{\partial \boldsymbol{n}_{\boldsymbol{x}}} = -\sum_{i,j=1}^{2} K_{ij} \frac{\partial T(\boldsymbol{x})}{\partial x_j} n_i(\boldsymbol{x}) = \bar{q}, \quad \boldsymbol{x} \in \Gamma_N, \tag{3}$$

$$\frac{\partial T(\boldsymbol{x})}{\partial \boldsymbol{n}_{\boldsymbol{x}}} = h_e(T(\boldsymbol{x}) - T_f), \quad \boldsymbol{x} \in \Gamma_R, \tag{4}$$

where $T(\boldsymbol{x})$ represents the temperature at the point $\boldsymbol{x}$, $K = \left\{K_{ij}(\boldsymbol{x},T)\right\}_{1\le i,j\le 2}$ the heat conduction coefficient matrix satisfying positive definite $(\Delta_K = \det(K) = K_{12}K_{21} - K_{11}K_{22} < 0)$ and symmetry $(K_{21} = K_{12})$ conditions, $\boldsymbol{n}_{\boldsymbol{x}}$ the unit outer normal vector at the boundary point $\boldsymbol{x}$, h_e the conductivity factor, T_f the ambient temperature. Γ_D, Γ_N and Γ_R denote boundary segments according to Dirichlet, Neumann and Robin boundaries, and $\Gamma = \Gamma_D + \Gamma_N + \Gamma_R$.

In this study, we focus on the exponentially functionally graded material whose heat conductivity matrix could be represented as follows

$$K_{ij}(\boldsymbol{x},T) = a(T)\bar{K}_{ij}e^{\sum_{i=1}^{2} 2\beta_i x_i}, \quad \boldsymbol{x} = (x_1, x_2) \in \Omega, \tag{5}$$

where $a(T) > 0$, β_1 and β_2 are the material parameters, $\bar{\boldsymbol{K}} = \left\{\bar{K}_{ij}\right\}_{1\le i,j\le 2}$ is a symmetric positive definite matrix.

By using the Kirchhoff transformation

$$\phi(T) = \int a(T)dT, \tag{6}$$

Equations (1)–(4) can be converted to

$$(\sum_{i,j=1}^{2}(\bar{K}_{ij}\frac{\partial^2 \Phi_T(\boldsymbol{x})}{\partial x_i \partial x_j} + 2\beta_i \bar{K}_{ij}\frac{\partial \Phi_T(\boldsymbol{x})}{\partial x_j}))e^{\sum_{i=1}^{2} 2\beta_i x_i} = 0, \quad \boldsymbol{x} \in \Omega, \tag{7}$$

$$\Phi_T(\boldsymbol{x}) = \phi(\bar{T}), \quad \boldsymbol{x} \in \Gamma_D, \tag{8}$$

$$q(\boldsymbol{x}) = -\sum_{i,j=1}^{2} K_{ij} \frac{\partial T(\boldsymbol{x})}{\partial x_j} n_i(\boldsymbol{x}) = -e^{\sum_{i=1}^{2} 2\beta_i x_i} \sum_{i,j=1}^{2} \bar{K}_{ij} \frac{\partial \Phi_T(\boldsymbol{x})}{\partial x_j} n_i(\boldsymbol{x}) = \bar{q}, \quad \boldsymbol{x} \in \Gamma_N, \tag{9}$$

$$q(\boldsymbol{x}) = h_e(\Phi_T(\boldsymbol{x}) - \varphi_T(\boldsymbol{x})), \quad \boldsymbol{x} \in \Gamma_R, \tag{10}$$

where $\Phi_T(\boldsymbol{x}) = \varphi(T(\boldsymbol{x}))$.

Let $\Phi_T = \Psi e^{-\sum_{i=1}^{2} \beta_i (x_i + s_i)}$, Eq (7) can be simplified to the following formula

$$\left(\sum_{i,j=1}^{2} \bar{K}_{ij} \frac{\partial \Psi(\boldsymbol{x})}{\partial x_i \partial x_j} - \lambda^2 \Psi(\boldsymbol{x})\right) e^{\sum_{i=1}^{2} \beta_i (x_i + s_i)} = 0, \quad \boldsymbol{x} \in \Omega, \tag{11}$$

where $\lambda = \sqrt{\sum_{i=1}^{2} \sum_{j=1}^{2} \beta_i \bar{K}_{ij} \beta_j}$, $\boldsymbol{s} = (s_1, s_2)$ is source point. Since $e^{\sum_{i=1}^{2} \beta_i (x_i + s_i)} > 0$, the above formula can degenerate into an anisotropic modified Helmholtz equation. Employing the following transformation

$$\begin{pmatrix} y_1 \\ y_2 \end{pmatrix} = \begin{pmatrix} 1/\sqrt{\bar{K}_{11}} & 0 \\ -\bar{K}_{12}/\sqrt{\bar{K}_{11}\Delta_{\bar{K}}} & \sqrt{\bar{K}_{11}}/\sqrt{\Delta_{\bar{K}}} \end{pmatrix} \begin{pmatrix} x_1 \\ x_2 \end{pmatrix}, \tag{12}$$

with $\Delta_{\bar{K}} = \det(\bar{K}) = \bar{K}_{11}\bar{K}_{22} - \bar{K}_{12}\bar{K}_{21} > 0$, an isotropic modified Helmholtz equation will be obtained, namely,

$$\sum_{i=1}^{2} \frac{\partial^2 \Psi(\boldsymbol{y})}{\partial^2 y_i} - \lambda^2 \Psi(\boldsymbol{y}) = 0, \quad \boldsymbol{y} \in \Omega. \tag{13}$$

The non-singular general solution of Eq (13) is available [49], and thus the non-singular general solution of Eq (11) can be derived by using the inverse transformation of Eq (12),

$$G(R) = -\frac{1}{2\pi\sqrt{\Delta_{\bar{k}}}} I_0(\lambda R), \tag{14}$$

where $R = \sqrt{\sum_{i=1}^{2} \sum_{j=1}^{2} r_i \bar{K}_{ij}^{-1} r_j}$, $r_1 = x_1 - s_1$, $r_2 = x_2 - s_2$, $\boldsymbol{x} = (x_1, x_2)$ and $\boldsymbol{s} = (s_1, s_2)$ are collocation node and source point, and I_0 indicates the zero-order modified Bessel function of first kind. Using the transform $\Phi_T = \Psi e^{-\sum_{i=1}^{2} \beta_i (x_i + s_i)}$ again, the non-singular general solution of Eq (7) is yielded, and written as

$$G(R) = -\frac{I_0(\lambda R)}{2\pi\sqrt{\Delta_{\bar{k}}}} e^{-\sum_{i=1}^{2} \beta_i (x_i + s_i)}. \tag{15}$$

3. Local knot method

This section will introduce the implementation of the LKM in solving Eq (7), with the help of the non-singular general solution (15). According to the basic theory of the LKM, $\left(\boldsymbol{x}_i\right)_{i=1}^{N}$ are discretized inside the domain Ω and along its boundary Γ, here $N=n_p+n_{b1}+n_{b2}+n_{b3}$, the numbers of boundary nodes satisfying the Dirichlet, Neumann and Robin boundary conditions are n_{b1}, n_{b2} and n_{b3}, respectively. n_p represents the number of interior nodes. Figure 1 shows the schematic diagram of the LKM, which indicates the distribution of the central node $\boldsymbol{x}^{(0)}$ and its m supporting points ($\boldsymbol{x}^{(p)}, p=1,2,...,m$) in a corresponding supporting domain Ω_s. For the $m+1$ local nodes inside the supporting domain Ω_s, we can express the unknown at the center node using a linear combination of the non-singular general solutions

$$\Phi(\boldsymbol{x}^{(p)})=\sum_{q=0}^{m}\alpha_q G(R_{pq}),\quad \boldsymbol{x}^{(p)}\in\Omega_s,\quad p=0,1,...,m, \tag{16}$$

or for brevity

$$\boldsymbol{\Phi}^{(p)}=\boldsymbol{G}^{(p)}\boldsymbol{\alpha}, \tag{17}$$

where $(\alpha_q)_{q=0}^{m}$ are the unknown coefficients, $G(R_{pq})$ is the non-singular general solution given in Eq (15).

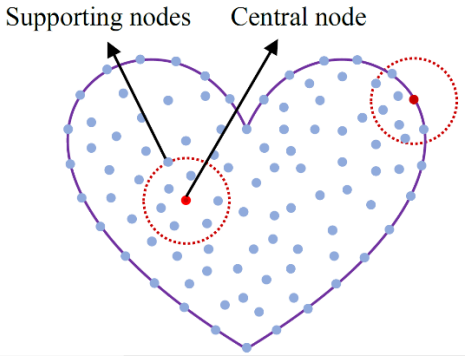

Figure 1. Two-dimensional schematic diagram of the LKM.

Based on the essential ideas of moving least squares (MLS) approximation, in each local subdomain, the residual function can be defined as follows

$$B(\Phi)=\sum_{p=0}^{m}\left[\boldsymbol{G}^{(p)}\boldsymbol{\alpha}-\boldsymbol{\Phi}^{(p)}\right]^2\omega^{(p)}, \tag{18}$$

where $\omega^{(p)}$ is the weight function, many kinds of weight functions can be adopted. We use the spline weight function [50] in the present study.

$$\omega^{(p)}=1-6\left(\frac{d_p}{d_{\max}}\right)^2+8\left(\frac{d_p}{d_{\max}}\right)^3-3\left(\frac{d_p}{d_{\max}}\right)^4,\quad p=0,1,...,m, \tag{19}$$

where d_p is the distance between the central node $\boldsymbol{x}^{(0)}$ and the pth supporting node $\boldsymbol{x}^{(p)}$, $d_{\max}$ is denotes the maximum value of distances between $\boldsymbol{x}^{(0)}$ and m supporting nodes, i.e., $d_{\max} = \max\limits_{p=1,2,...,m}(d_p)$.

On the basis of the MLS theory, the undetermined coefficients $\boldsymbol{\alpha} = (\alpha_0, \alpha_1, ..., \alpha_m)^T$ could be decided by minimizing the functional $B(\Phi)$, namely,

$$\frac{\partial B(\Phi)}{\partial \alpha_q} = 0, \quad q = 0,1,...,m. \tag{20}$$

From Eq (20), the following linear system can be consisted

$$\boldsymbol{A}\boldsymbol{\alpha} = \boldsymbol{b}, \tag{21}$$

where

$$\boldsymbol{A} = \begin{bmatrix} \sum\limits_{p=0}^{m} G_{p0}^2\omega^{(p)} & \sum\limits_{p=0}^{m} G_{p0}G_{p1}\omega^{(p)} & \sum\limits_{p=0}^{m} G_{p0}G_{p2}\omega^{(p)} & \cdots & \sum\limits_{p=0}^{m} G_{p0}G_{pm}\omega^{(p)} \\ & \sum\limits_{p=0}^{m} G_{p1}^2\omega^{(p)} & \sum\limits_{p=0}^{m} G_{p1}G_{p2}\omega^{(p)} & \cdots & \sum\limits_{p=0}^{m} G_{p1}G_{pm}\omega^{(p)} \\ & & \sum\limits_{p=0}^{m} G_{p2}^2\omega^{(p)} & \cdots & \sum\limits_{p=0}^{m} G_{p2}G_{pm}\omega^{(p)} \\ & \text{SYM} & & \ddots & \vdots \\ & & & & \sum\limits_{p=0}^{m} G_{pm}^2\omega^{(p)} \end{bmatrix}, \ \boldsymbol{b} = \begin{bmatrix} \sum\limits_{p=0}^{m} G_{p0}\omega^{(p)}\Phi^{(p)} \\ \sum\limits_{p=0}^{m} G_{p1}\omega^{(p)}\Phi^{(p)} \\ \sum\limits_{p=0}^{m} G_{p2}\omega^{(p)}\Phi^{(p)} \\ \vdots \\ \sum\limits_{p=0}^{m} G_{pm}\omega^{(p)}\Phi^{(p)} \end{bmatrix}. \tag{22}$$

The unknown vector $\boldsymbol{b}$ in Eq (22) could be recast as

$$\boldsymbol{b} = \begin{bmatrix} G_{00}\omega^{(0)} & G_{10}\omega^{(1)} & \cdots & G_{m0}\omega^{(m)} \\ G_{01}\omega^{(0)} & G_{11}\omega^{(1)} & \cdots & G_{m1}\omega^{(m)} \\ \vdots & \vdots & \ddots & \vdots \\ G_{0m}\omega^{(0)} & G_{1m}\omega^{(1)} & \cdots & G_{mm}\omega^{(m)} \end{bmatrix} \begin{pmatrix} \Phi^{(0)} \\ \Phi^{(1)} \\ \vdots \\ \Phi^{(m)} \end{pmatrix} = \boldsymbol{B} \begin{pmatrix} \Phi^{(0)} \\ \Phi^{(1)} \\ \vdots \\ \Phi^{(m)} \end{pmatrix}. \tag{23}$$

In accordance with Eqs (21)–(23), the coefficient vector $\boldsymbol{\alpha} = (\alpha_0, \alpha_1, ..., \alpha_m)^T$ can be repressed as

$$\boldsymbol{\alpha} = \begin{bmatrix} \alpha_0 \\ \vdots \\ \alpha_m \end{bmatrix} = \boldsymbol{A}^{-1}\boldsymbol{B} \begin{pmatrix} \Phi^{(0)} \\ \Phi^{(1)} \\ \vdots \\ \Phi^{(m)} \end{pmatrix}. \tag{24}$$

Substituting Eq (24) into Eq (17) as $p = 0$, the temperature at central node $\boldsymbol{x}^{(0)}$ is expressed as

$$\Phi^{(0)} = \boldsymbol{G}^{(0)}\boldsymbol{\alpha} = \boldsymbol{G}^{(0)}\boldsymbol{A}^{-1}\boldsymbol{B}\begin{pmatrix}\Phi^{(0)}\\ \Phi^{(1)}\\ \vdots\\ \Phi^{(m)}\end{pmatrix} = \sum_{q=0}^{m} f^{(q)}\Phi^{(q)}, \tag{25}$$

or

$$\Phi^{(0)} - \sum_{q=0}^{m} f^{(q)}\Phi^{(q)} = 0, \tag{26}$$

in which $(f^{(q)})_{q=0}^{m} = \boldsymbol{G}^{(0)}\boldsymbol{A}^{-1}\boldsymbol{B}$. Follow the above process, the unknowns $\Phi(\boldsymbol{x}_i)$ at all nodes $(\boldsymbol{x}_i)_{i=1}^{N}$ can be expressed in the form of Eq (26).

In addition, the normal heat flux at the boundary node can be calculated by

$$\frac{\partial \Phi^{(0)}}{\partial \boldsymbol{n}_{\boldsymbol{x}^{(0)}}} = \sum_{q=0}^{m} \boldsymbol{\alpha}_q Q(\boldsymbol{x}^{(0)}, \boldsymbol{x}^{(q)}) = Q(\boldsymbol{x}^{(0)}, \boldsymbol{x}^{(q)})\boldsymbol{A}^{-1}\boldsymbol{B}\begin{pmatrix}\Phi^{(0)}\\ \Phi^{(1)}\\ \vdots\\ \Phi^{(m)}\end{pmatrix}, \tag{27}$$

in which

$$\begin{aligned} Q(\boldsymbol{x}^{(0)}, \boldsymbol{x}^{(q)}) &= \sum_{i,j=1}^{2} \bar{K}_{ij} \frac{\partial G(\boldsymbol{x}^{(0)}, \boldsymbol{x}^{(q)})}{\partial x_j^{(0)}} n_i(\boldsymbol{x}^{(0)}) e^{\sum_{i=1}^{2} 2\beta_i x_i^{(0)}} \\ &= \frac{e^{\sum_{i=1}^{2} 2\beta_i r_i}}{2\pi\sqrt{\Delta_{\bar{K}}}}\left(-\frac{\lambda}{R_{0q}} I_1(\lambda R_{0q}) \sum_{i=1}^{2} n_i(\boldsymbol{x}^{(0)}) r_i + I_0(\lambda R_{0q}) \sum_{i=1}^{2}\sum_{j=1}^{2} n_i(\boldsymbol{x}^{(0)}) \bar{K}_{ij}\beta_j\right), \end{aligned} \tag{28}$$

or for brevity

$$\frac{\partial \Phi^{(0)}}{\partial \boldsymbol{n}_{\boldsymbol{x}^{(0)}}} = \sum_{l=0}^{m} e^{(l)}\Phi^{(l)}, \tag{29}$$

where $(e^{(l)})_{l=0}^{m} = Q(\boldsymbol{x}^{(0)}, \boldsymbol{x}^{(q)})\boldsymbol{A}^{-1}\boldsymbol{B}$. If the central node $\boldsymbol{x}^{(0)}$ is a boundary node with Robin boundary condition, we have

$$\frac{\partial \Phi^{(0)}}{\partial \boldsymbol{n}_{\boldsymbol{x}^{(0)}}} = h_e(\Phi^{(0)} - \varphi^{(0)}), \tag{30}$$

Substituting Eq (29) into Eq (30) yields

$$\sum_{l=0}^{m} e^{(l)}\Phi^{(l)} = h_e(\Phi^{(0)} - \varphi^{(0)}). \tag{31}$$

For the interior nodes, the temperature distribution should satisfy Eq (26), namely,

$$\Phi^{(p)} - \sum_{q=0}^{m} f_p^{(q)}\Phi^{(q)} = 0, \quad p = 1, 2, ..., n_p, \tag{32}$$

where the subscript p of $f_p^{(q)}$ is a coefficient used to differentiate the different internal nodes. For the

boundary nodes satisfying Dirichlet boundary conditions, the following equation should be satisfied

$$\Phi^{(p)} = \bar{\Phi}^{(p)}, \quad p = n_p + 1, n_p + 2, ..., n_p + n_{b1}. \tag{33}$$

For the boundary nodes with Neumann conditions, we have

$$\sum_{l=0}^{m} e_p^{(l)} \Phi^{(l)} = \bar{q}(\boldsymbol{x}^{(p)}), \quad p = n_p + n_{b1} + 1, n_p + n_{b1} + 2, ..., n_p + n_{b1} + n_{b2}. \tag{34}$$

For the boundary nodes with Robin conditions, we have

$$h_e \Phi^{(p)} - \sum_{l=0}^{m} e_p^{(l)} \Phi^{(l)} = h\varphi^{(p)}, \quad p = n_p + n_{b1} + n_{b2} + 1, n_p + n_{b1} + n_{b2} + 2, ..., N. \tag{35}$$

In Eqs (34) and (35), the subscript "p" (indicates the node number) is used to distinguish the different boundary nodes.

By using given boundary data and combining Eqs (32)–(35), the following sparse system of linear equations is obtained

$$\boldsymbol{A}\boldsymbol{\Phi}_T = \boldsymbol{b}, \tag{36}$$

in which $\boldsymbol{A}_{N\times N}$ is the matrix of coefficient, $\boldsymbol{\Phi}_T = \left[\Phi^{(1)}, \Phi^{(2)}, ..., \Phi^{(N)}\right]^T$ represents the unascertained vector of variables at all nodes, and $\boldsymbol{b}_{N\times 1}$ denotes the known vector. After obtaining the solution $\boldsymbol{\Phi}_T$ of Eq (36), the solution of the original problem (Eq (1)) can be acquired by using the inverse Kirchhoff transformation

$$T(\boldsymbol{x}) = \varphi^{-1}(\Phi_T(\boldsymbol{x})). \tag{37}$$

To summarize and to make clearer the procedure of the developed method for solving the heat conduction problem in nonlinear functionally graded material, a computational flow chart is given in Figure 2.

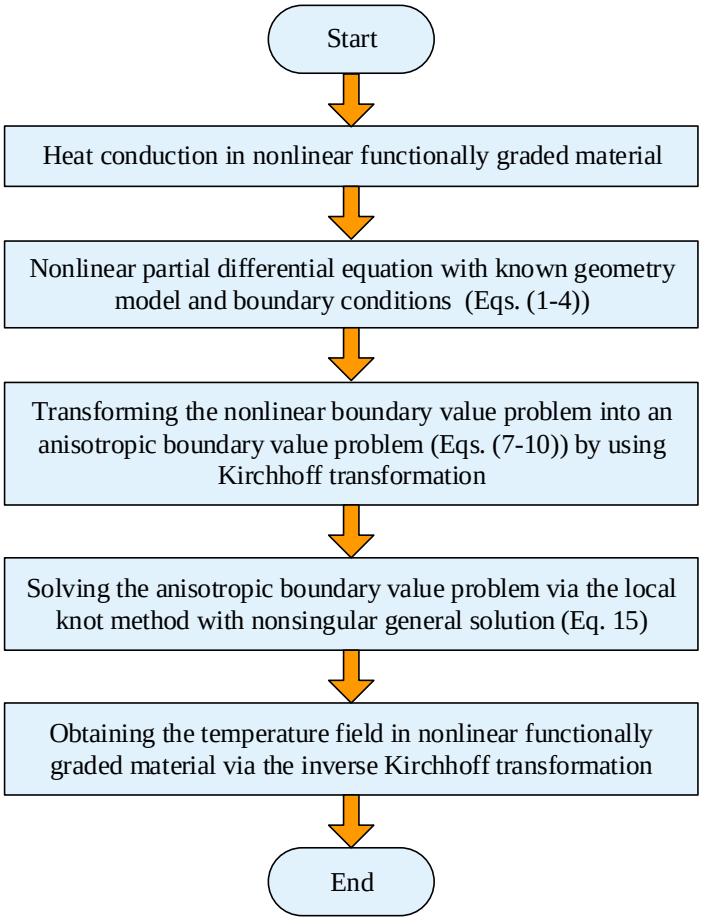

Figure 2. Computational flow chart.

4. Numerical examples

In this section, three typical numerical examples are provided to verify the applicability and accuracy of the proposed method for solving the heat conduction problem of two-dimensional nonlinear functionally graded materials. In order to estimate the accuracy, the measured errors are defined as

$$\text{Global error} = \sqrt{\sum_{k=1}^{W}\left(u_n^k - u_e^k\right)^2} \Big/ \sqrt{\sum_{k=1}^{W}\left(u_e^k\right)^2}, \tag{38}$$

$$\text{Max error} = \max\left\{\left|u_n^k - u_e^k\right|\right\}, \tag{39}$$

where W is the number of all test points, u_n^k and u_e^k are numerical and analytical solutions at test points, respectively. Remarkably, all the calculations were done on a laptop (Intel® CoreTMi5-9300H CPU at 2.40 GHz, 8G RAM) by using the MATLAB program.

4.1. Example 1

The typical heat transfer problem of exponential heterogeneous gradient materials is considered.

In a high-temperature environment, the coefficient of heat conduction is defined as $a(T)=e^{T}$. We can acquire $\Phi_T=e^{T}$, $T=\varphi^{-1}(\Phi_T)=\ln(\Phi_T)$ by the Kirchhoff transformation. Here, we consider a square domain $\Omega=[-1,1]\times[-1,1]$ of orthotropic material with $\bar{K}=\begin{pmatrix}2 & 0\\ 0 & 1\end{pmatrix}$ and $\beta_1=0$, $\beta_2=1$. The lower and right boundaries of the structure respectively satisfy the Dirichlet and Neumann boundary conditions, and the other boundaries satisfy the Robin boundary condition. The analytical solution is

$$T(x)=\ln\left(\sqrt{\frac{1-Tx/Tr}{2Tr}}\sinh(Tr)e^{-Ty}\right), \tag{40}$$

where $Tx=x_1/\sqrt{2}-1$, $Ty=x_2$, and $Tr=\sqrt{Tx^2+Ty^2}$.

For the sake of investigating the influence of the total number of nodes on the calculation results, 2300 regular and irregular nodes are used in the calculation (as shown in Figure 3). Irregular nodes are derived by jiggling the regular nodes, i.e., assigning a perturbation on regular nodes along the *x* and *y* directions. The temperature distribution in the domain can be calculated with different numbers of supporting node ($10\le m\le 40$). Figure 4 shows the error curves as the number of supporting node increases, under regular/irregular nodal distributions. As can be seen from Figure 4, although the errors show fluctuation for some specific numbers of supporting node, it can still be seen that the global errors and the maximum errors generally have a decreasing trend with the increase of supporting nodes. In this example, $m=35$ is a relatively optimal value to achieve the highest accuracy. This indicates that the number of supporting nodes has a certain influence on the calculation results, but a relatively ideal numerical result can be obtained in a larger range.

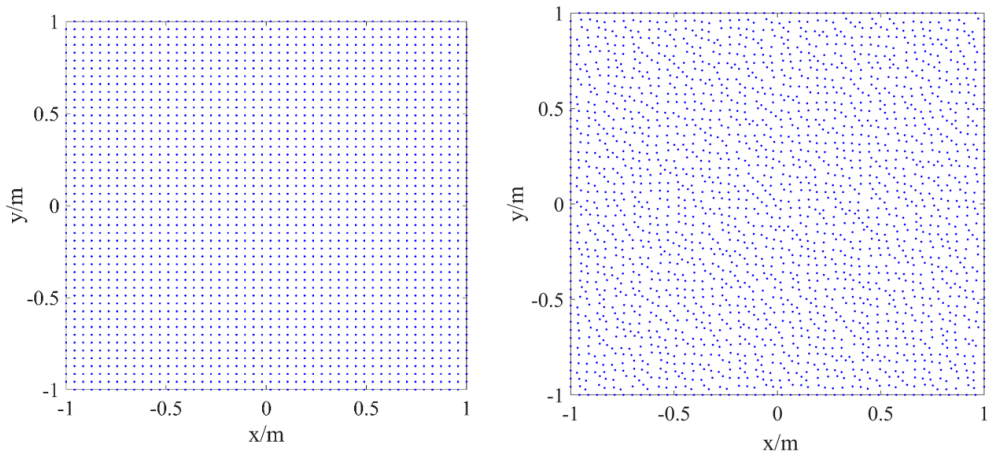

Figure 3. Distributions of nodes: (a) Regular nodes; (b) Irregular nodes.

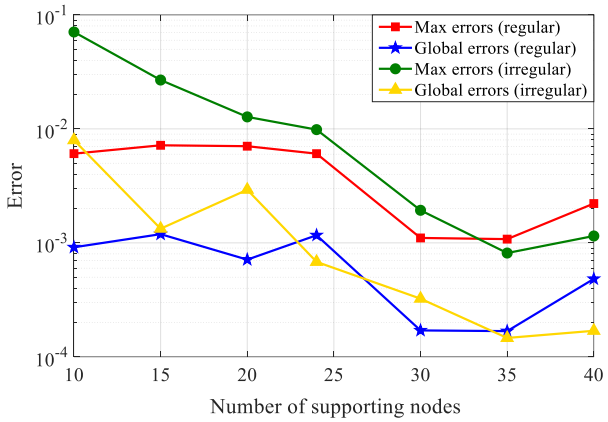

Figure 4. Error curves of the LKM with respect to the number of supporting nodes, under regular and irregular distributions of nodes.

In fact, the number of supporting nodes (m) is related to the node spacing ($\Delta h = \max\limits_{1\le i\le N} \min\limits_{1\le j\le N} \left| \boldsymbol{x}_i - \boldsymbol{x}_j \right|$). In order to numerically analyze the relationship between m and Δh, we investigate the global errors under different values of m and Δh. Figure 5 displays the 3D error surface and the 2D error plane. The red dots in Figure 5(b) indicate the positions of Global error $=10^{-3}$. Using the curve fitting method, we can obtain an estimation formula that ensures the global error is almost equal to 10^{-3}, $m = \lceil 0.02297 \cdot \Delta h^{(-1.885)} \rceil$, where $\lceil \cdot \rceil$ denotes the round up operation. Furthermore, the positions corresponding to the relatively optimal value of m are plotted by white squares. In the same way, the relatively optimal value of m can be formulated by

$$m = \lceil 0.6387 \cdot \Delta h^{(-1.213)} \rceil. \tag{41}$$

According to Eq (41), we can easily estimate the number of supported nodes according to the node spacing. This example uses 2300 nodes, and thus Δh is about 0.038. It can be observed from Figure 5(b) that Global error $\le 10^{-3}$ when $10 \le m \le 40$.

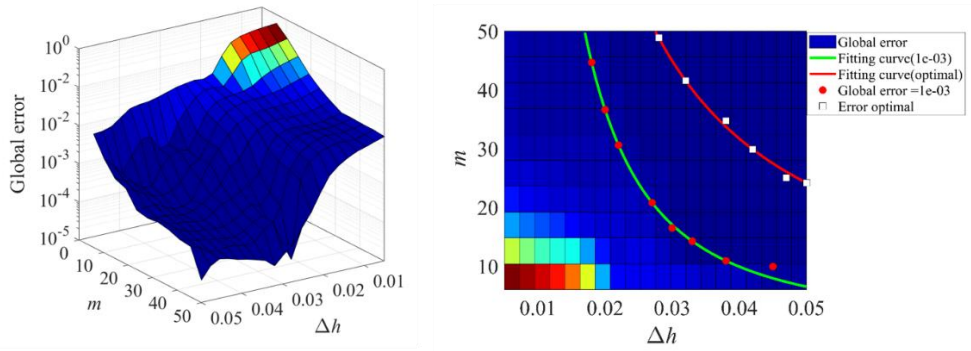

(a) 3D error surface (b) 2D error plane

Figure 5. Distributions of global errors under different values of m and Δh.

Figure 6 shows the variations of errors with the increase of the total number of nodes under the regular and irregular nodes, where $m = 30$. We can observe that both the maximum errors and global errors are less than 5.621×10^{-2}, and both decrease with the augment of the total number of nodes, indicating that the LKM has the good accuracy and convergence in dealing with the heat transfer problem of nonlinear functionally graded materials. It can also be obtained from Figure 6 that the calculation precision with regular node distribution is higher than that with irregular node distribution, which verifies that the proposed method, as a local meshless method, can simulate the heat conduction problem with arbitrary node distribution, and the calculation accuracy with regular node distribution is slightly better.

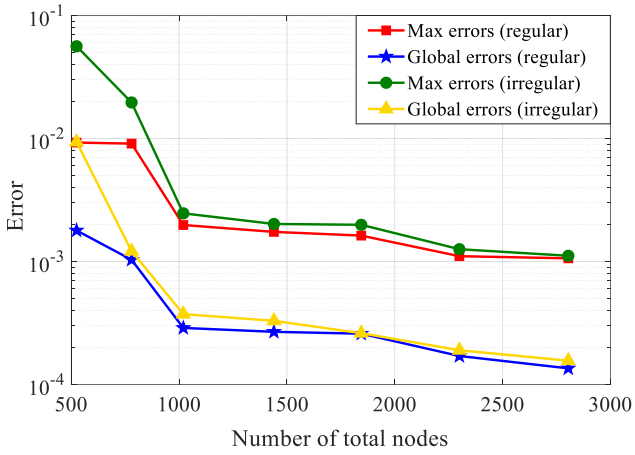

Figure 6. Error curves of the LKM with respect to the total number of nodes, under regular and irregular distributions of nodes.

In the case of regular nodes, Figure 7 displays the distributions of the exact solution and absolute error in the calculation domain. From Figure 7, we can clearly observe that the LKM can reach a higher precision, and the absolute error is less than 1.104×10^{-3}.

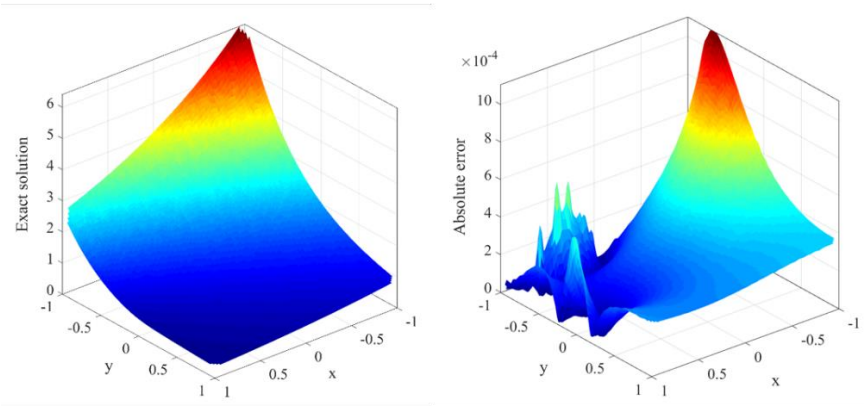

(a) Exact solution (b) Absolute error

Figure 7. Comparison of numerical results in the calculation domain: (a) Exact solution; (b) Absolute error.

To validate the accuracy and condition number of the developed method, we compared the LKM with the BKM. Table 1 lists the errors and the condition numbers of the above two methods with increasing number of boundary nodes. It is worth noting that the BKM is a boundary meshless method, while the LKM is a local meshless method. In the BKM, the number of boundary nodes (*NB*) is set to the same value as the LKM to ensure the fairness of comparison. From Table 1, it is observed that the numerical veracity of the LKM is marginally better than that of the BKM for various values of *NB*. Moreover, the condition number of the LKM is obviously less than that of the BKM. It could be carefully concluded that the presented LKM is accurate and stable for solving two-dimensional nonlinear heat conduction problems.

Table 1. Comparison of numerical results acquired by the LKM and the BKM under different numbers of boundary nodes.

NB	BKM			LKM		
	Max Error	Global Error	Cond(A)	Max Error	Global Error	Cond(A)
116	1.783×10^{-3}	1.069×10^{-3}	1.575e+19	1.063×10^{-3}	1.589×10^{-4}	2.958e+03
216	2.011×10^{-3}	1.257×10^{-3}	2.039e+20	1.366×10^{-3}	2.064×10^{-4}	2.458e+04
320	1.900×10^{-3}	1.232×10^{-3}	1.229e+20	1.840×10^{-3}	1.970×10^{-4}	2.908e+05
404	1.876×10^{-3}	1.131×10^{-3}	1.043e+20	1.583×10^{-3}	1.353×10^{-4}	1.977e+07

4.2. Example 2

The second example considers a heat transfer problem on a square functionally graded material plate with four circular holes of the same size, as shown in Figure 8(a). The temperatures are assumed to be known on the boundaries **a** and **b**, the heat fluxes are given on the boundaries **c** and **d**, and the boundaries of four circular holes are adiabatic. The relevant parameters are set as: $L=1.0$, $L_1=0.3$, $L_2=0.2$, $r=0.1$. In fact, the thermal conductivity can be expressed as a linear relationship with temperature.

The exact solution is indicated as

$$T(x)=\frac{-1+\sqrt{1+2\mu\Phi_T(x)}}{\mu}. \tag{42}$$

Using the Kirchhoff transformation, we can get

$$\Phi_T(x)=e^{\lambda(Tx+Ty)/\tau-\sum_{i=1}^{2}\beta_i x_i}, \tag{43}$$

where $\mu=1/4$, $Tx=\frac{x_1\sqrt{\Delta_{\bar{K}}}}{\bar{K}_{11}}$, $Ty=-\frac{x_1\bar{K}_{12}}{\bar{K}_{11}}+x_2$, $\tau=\sqrt{\bar{K}_{11}(\frac{\sqrt{\Delta_{\bar{K}}}-\bar{K}_{12}}{\bar{K}_{11}})^2+2\bar{K}_{12}(\frac{\sqrt{\Delta_{\bar{K}}}-\bar{K}_{12}}{\bar{K}_{11}})+\bar{K}_{22}}$.

$\bar{K}=\begin{pmatrix}1 & 0.25\\ 0.25 & 3\end{pmatrix}$, $\beta_1=0.1$, $\beta_2=0.8$.

Under $N=1226$ (as shown in Figure 8(b)) and $m=60$, Figure 9 illustrates the comparison of numerical results on the computational domain. It can be found from the figure that the numerical results obtained by the LKM are extremely in agreement with the analytical solutions. Furthermore,

the absolute errors are less than 8.306×10^{-5}, and the maximum error appears at the boundary **d**. It can be seen from Table 2, both global errors and maximum errors decrease with increasing number of supporting node, showing a convergence trend. As can be expected, the CPU times gradually increase with increasing number of supporting nodes, but not too much even for the relatively larger value $m=60$.

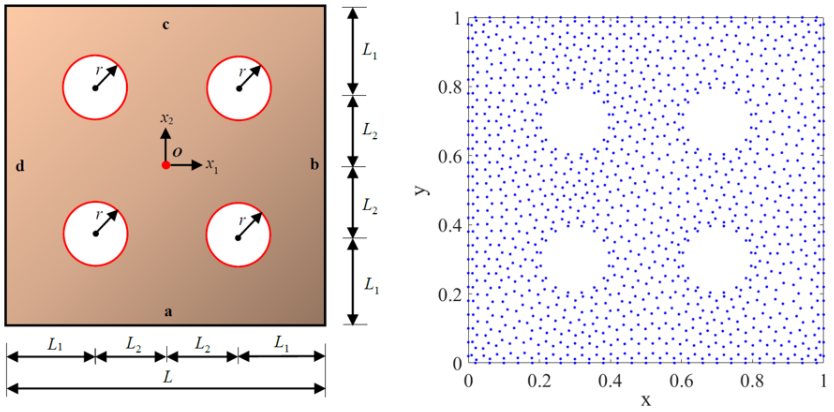

(a) A geometric model (b) Nodal distribution

Figure 8. A geometric model and nodal distribution of a plate.

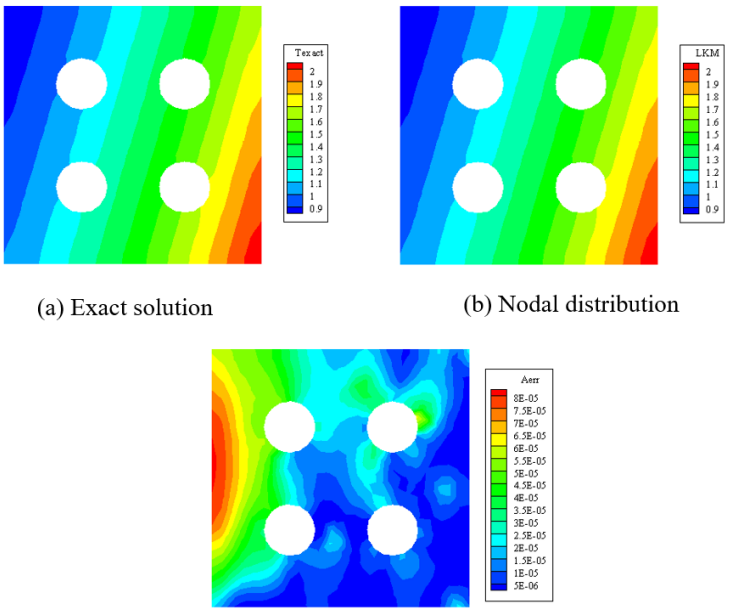

(a) Exact solution (b) Nodal distribution

(c) Absolute error

Figure 9. Profiles of temperature and error on the plate: (a) Exact solution; (b) LKM; (c) Absolute error.

Table 2. Global errors, Max errors and CPU times with the increase of the number of supporting nodes, where $N = 1266$.

m	20	30	40	50	60
Global errors	2.643e-03	1.661e-04	1.407e-04	6.967e-05	2.381e-05
Max errors	7.528e-03	9.004e-04	6.408e-04	2.620e-04	8.306e-05
CPU times (s)	1.134	1.412	2.052	2.868	3.659

Finally, we set $m = 60$, Figure 10 depicts the absolute errors of the LKM under different numbers ($N = 960,\ 1890,\ 2620$) of total nodes. Noted that the error becomes smaller and smaller as the number of total nodes increases, indicating a convergence trend. The above numerical experiment with complicated geometries and mixed boundary conditions confirms the capacity, accuracy, and convergence of the developed methodology in solving the 2D heat conduction in nonlinear functionally graded material.

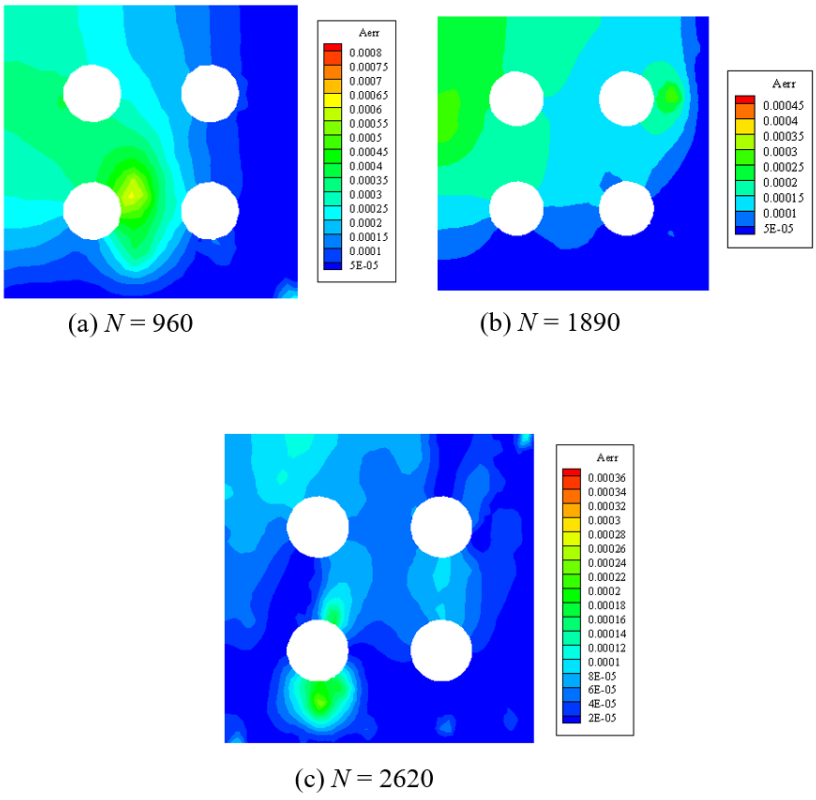

(a) $N = 960$ (b) $N = 1890$

(c) $N = 2620$

Figure 10. Comparison of numerical results on the computational domain, under different numbers of total nodes: (a) $N = 960$; (b) $N = 1890$; (c) $N = 2620$.

4.3. Example 3

In the last example, the LKM is applied to a nonlinear heat conduction problem in an irregular

domain. Figure 11 shows the geometry model of the problem. In this case, we use the same analytical solution and parameters as for example 2.

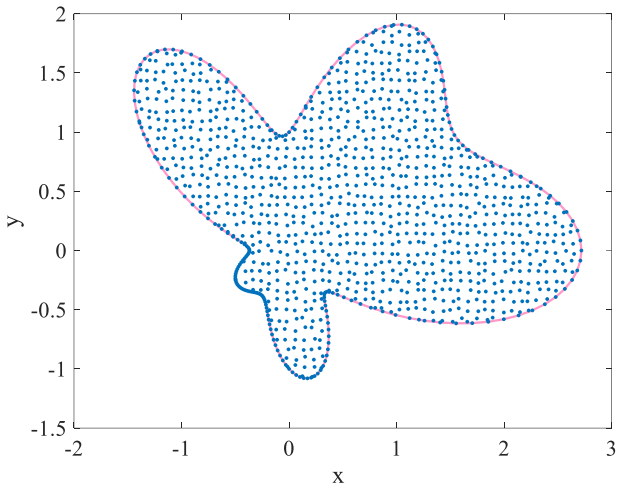

Figure 11. Nodal distribution in an amoeba-like domain.

To investigate the influence of the number of supporting nodes on the computational accuracy, we set N to be 1228 (irregular nodes) and plot the relative errors of the temperatures at all points in Figure 12, when m is equal to 30, 40, and 50. It is noticed that the error gradually decreases with increasing number of supporting nodes.

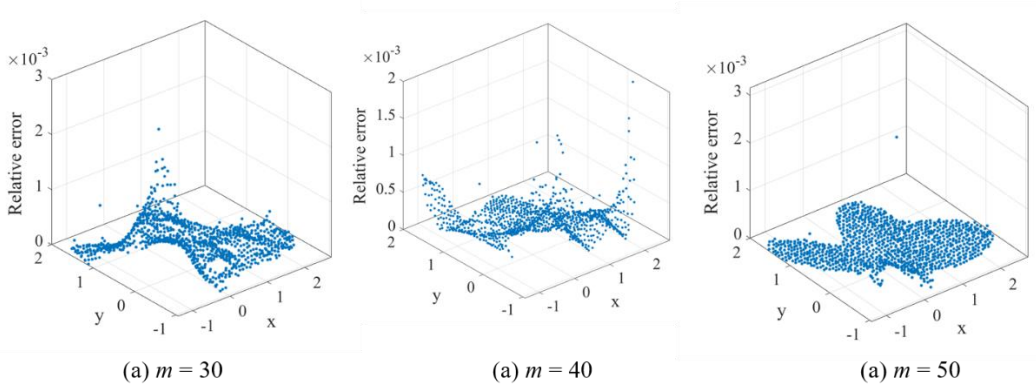

Figure 12. Relative errors of the temperatures at all nodes, under different numbers of supporting nodes: (a) $m = 30$; (b) $m = 40$; (c) $m = 50$.

To investigate the convergence of the LKM for nonlinear heat conduction problem in an irregular structure, Figure 13 shows the variations of global errors and maximum errors as the increase of node number. Numerical results in the figure demonstrate the good convergence properties of the proposed scheme. Furthermore, even if the number of nodes exceeds 100000, the numerical simulation work is still performed on a regular laptop. A great number of numerical tests indicate that the proposed methodology in this paper is accurate, stable and convergent, and is suitable for large-scale simulations in an arbitrary domain.

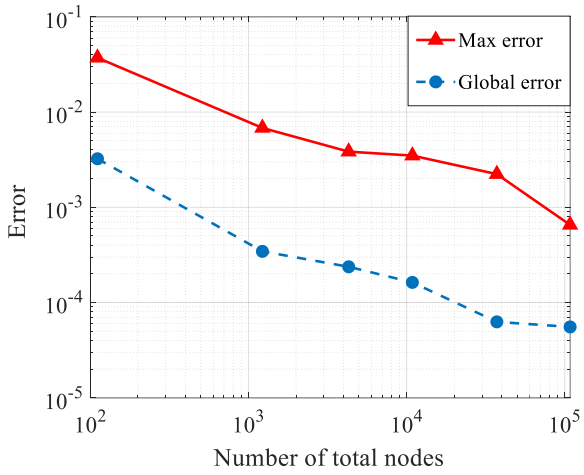

Figure 13. Error curves of the LKM with respect to the number of total nodes.

5. Conclusions

This paper firstly presented a novel local semi-analytical meshless method, the local knot method (LKM) in conjunction with the Kirchhoff transformation, to numerically simulate heat conduction problems of nonlinear functionally graded materials. As a local semi-analytical meshless algorithm, the LKM uses the non-singular general solution as the basis function. Compared with the traditional BKM, this method not only retains the simplicity and high accuracy, but also avoids an ill-conditioned system of equations, and is more appropriate for large-scale simulations associated with complex structures.

Numerical experiments including simply/multi-connected and regular/irregular domains shown that the proposed method is accurate, stable, and convergent. Furthermore, the resultant matrix is well-conditioned and has a smaller condition number than the traditional BKM. Compared with the existing methods for solving the heat conduction problem of nonlinear functionally graded materials, the present scheme could be regarded as a highly competitive one.

Acknowledgments

The work described in this paper was supported by the National Natural Science Foundation of China (No.11802151), the Natural Science Foundation of Shandong Province of China (No. ZR2019BA008), and the China Postdoctoral Science Foundation (No. 2019M652315).

Conflict of interest

The authors declare that they have no conflicts of interest to report regarding the present study.

References

1. L. L. Cao, Q. H. Qin, N. Zhao, Hybrid graded element model for transient heat conduction in functionally graded materials, *Acta Mech. Sin.*, **28** (2012), 128–139.

2. A. Lal, H. N. Singh, N. L. Shegokar, FEM model for stochastic mechanical and thermal postbuckling response of functionally graded material plates applied to panels with circular and square holes having material randomness, *Int. J. Mech. Sci.*, **62** (2012), 18–33.
3. S. Akbarpour, H. R. Motamedian, A. Abedian, Micromechanical fem modeling of thermal stresses in functionally graded materials, In: *ICAS Secretariat - 26th Congress of International Council of the Aeronautical Sciences 2008*, ICAS 2008, 2008, 2851–2859.
4. Y. Chai, W. Li, Z. Liu, Analysis of transient wave propagation dynamics using the enriched finite element method with interpolation cover functions, *Appl. Math. Comput.*, **412** (2022), 126564.
5. A. Sutradhar, G. H. Paulino, The simple boundary element method for transient heat conduction in functionally graded materials, *Comput. Method. Appl. M.*, **193** (2004), 4511–4539.
6. M. I. Azis, D. L. Clements, Nonlinear transient heat conduction problems for a class of inhomogeneous anisotropic materials by BEM, *Eng. Anal. Bound. Elem.*, **32** (2008), 1054–1060.
7. M. Tanaka, T. Matsumoto, Y. Suda, S. Takakuwa, A dual reciprocity time-stepping BEM applied to the transient heat conduction problem of functionally graded materials, *Transactions of the Japan Society of Mechanical Engineers Series A*, **68** (2002), 1702–1707.
8. B. L. Wang, Z. H. Tian, Application of finite element–finite difference method to the determination of transient temperature field in functionally graded materials, *Finite Elem. Anal. Des.*, **41** (2005), 335–349.
9. C. Wang, Z. P. Qiu, Interval finite difference method for steady-state temperature field prediction with interval parameters, *Acta Mech. Sin.*, **30** (2014), 161–166.
10. C. Wang, Z. P. Qiu, Fuzzy finite difference method for heat conduction analysis with uncertain parameters, *Acta Mech. Sin.*, **30** (2014), 383–390.
11. W. Li, Q. Zhang, Q. Gui, Y. Chai, A coupled FE-meshfree triangular element for acoustic radiation problems, *Int. J. Comput. Meth.*, **18** (2020), 2041002.
12. S. S. Saliba, L. Gori, R. L. Pitangueira, A coupled finite element-meshfree smoothed point interpolation method for nonlinear analysis, *Eng. Anal. Bound. Elem.*, **128** (2021), 1–18.
13. V. Sladek, J. Sladek, M. Tanaka, C. Zhang, Transient heat conduction in anisotropic and functionally graded media by local integral equations, *Eng. Anal. Bound. Elem.*, **29** (2005), 1047–1065.
14. J. Sladek, V. Sladek, C. Hellmich, J. Eberhardsteiner, Heat conduction analysis of 3-D axisymmetric and anisotropic FGM bodies by meshless local Petrov–Galerkin method, *Comput. Mech.*, **39** (2007), 323–333.
15. A. R. Ahmad, A. Bagri, S. Bordas, T. Rabczuk, Analysis of thermoelastic waves in a two-dimensional functionally graded materials domain by the meshless local Petrov-Galerkin (MLPG) method, *CMES-Computer Modeling in Engineering & Sciences*, **65** (2010), 27–74.
16. Y. Wang, Y. Gu, J. Liu, A domain-decomposition generalized finite difference method for stress analysis in three-dimensional composite materials, *Appl. Math. Lett.*, **104** (2020), 106226.
17. W. Qu, H. He, A spatial–temporal GFDM with an additional condition for transient heat conduction analysis of FGMs, *Appl. Math. Lett.*, **110** (2020), 106579.
18. Q. Zhao, C. M. Fan, F. Wang, W. Qu, Topology optimization of steady-state heat conduction structures using meshless generalized finite difference method, *Eng. Anal. Bound. Elem.*, **119** (2020), 13–24.
19. P. W. Li, Space–time generalized finite difference nonlinear model for solving unsteady Burgers' equations, *Appl. Math. Lett.*, **114** (2021), 106896.

20. F. Wang, W. Chen, C. Zhang, J. Lin, Analytical evaluation of the origin intensity factor of time-dependent diffusion fundamental solution for a matrix-free singular boundary method formulation, *Appl. Math. Model.*, **49** (2017), 647–662.
21. Z. Fu, W. Chen, P. Wen, C. Zhang, Singular boundary method for wave propagation analysis in periodic structures, *J. Sound Vib.*, **425** (2018), 170–188.
22. X. Wei, W. Luo, 2.5D singular boundary method for acoustic wave propagation, *Appl. Math. Lett.*, **112** (2021), 106760.
23. L. Qiu, F. Wang, J. Lin, A meshless singular boundary method for transient heat conduction problems in layered materials, *Comput. Math. Appl.*, **78** (2019), 3544–3562.
24. F. Wang, W. Chen, Q. Hua, A simple empirical formula of origin intensity factor in singular boundary method for two-dimensional Hausdorff derivative Laplace equations with Dirichlet boundary, *Comput. Math. Appl.*, **76** (2018), 1075–1084.
25. Z. J. Fu, W. Chen, Q. H. Qin, Boundary knot method for heat conduction in nonlinear functionally graded material, *Eng. Anal. Bound. Elem.*, **35** (2011), 729–734.
26. Z. J. Fu, J. H. Shi, W. Chen, L. W. Yang, Three-dimensional transient heat conduction analysis by boundary knot method, *Math. Comput. Simulat.*, **165** (2019), 306–317.
27. C. M. Fan, Y. K. Huang, P. W. Li, Y. T. Lee, Numerical solutions of two-dimensional stokes flows by the boundary knot method, *CMES-Computer Modeling in Engineering and Sciences*, **105** (2015), 491–515.
28. L. Sun, C. Zhang, Y. Yu, A boundary knot method for 3D time harmonic elastic wave problems, *Appl. Math. Lett.*, **104** (2020), 106210.
29. H. Wang, Q. H. Qin, Y. L. Kang, A meshless model for transient heat conduction in functionally graded materials, *Comput. Mech.*, **38** (2006), 51–60.
30. L. Marin, D. Lesnic, The method of fundamental solutions for nonlinear functionally graded materials, *Int. J. Solids Struct.*, **44** (2007), 6878–6890.
31. G. Fairweather, A. Karageorghis, The method of fundamental solutions for elliptic boundary value problems, *Adv. Comput. Math.*, **9** (1998), 69–95.
32. F. Wang, C. S. Liu, W. Qu, Optimal sources in the MFS by minimizing a new merit function: Energy gap functional, *Appl. Math. Lett.*, **86** (2018), 229–235.
33. C. M. Fan, Y. K. Huang, C. S. Chen, S. R. Kuo, Localized method of fundamental solutions for solving two-dimensional Laplace and biharmonic equations, *Eng. Anal. Bound. Elem.*, **101** (2019), 188–197.
34. F. Wang, Y. Gu, W. Qu, C. Zhang, Localized boundary knot method and its application to large-scale acoustic problems, *Comput. Method. Appl. M.*, **361** (2020), 112729.
35. X. Yue, F. Wang, C. Zhang, H. Zhang, Localized boundary knot method for 3D inhomogeneous acoustic problems with complicated geometry, *Appl. Math. Model.*, **92** (2021), 410–421.
36. W. Qu, C. M. Fan, Y. Gu, F. Wang, Analysis of three-dimensional interior acoustic fields by using the localized method of fundamental solutions, *Appl. Math. Model.*, **76** (2019), 122–132.
37. Y. Gu, C. M. Fan, R. P. Xu, Localized method of fundamental solutions for large-scale modeling of two-dimensional elasticity problems, *Appl. Math. Lett.*, **93** (2019), 8–14.
38. F. Wang, C. M. Fan, Q. Hua, Y. Gu, Localized MFS for the inverse Cauchy problems of two-dimensional Laplace and biharmonic equations, *Appl. Math. Comput.*, **364** (2020), 124658.
39. X. Li, S. Li, On the augmented moving least squares approximation and the localized method of fundamental solutions for anisotropic heat conduction problems, *Eng. Anal. Bound. Elem.*, **119** (2020), 74–82.

40. Y. Gu, C. M. Fan, W. Qu, F. Wang, Localized method of fundamental solutions for large-scale modelling of three-dimensional anisotropic heat conduction problems – Theory and MATLAB code, *Comput. Struct.*, **220** (2019), 144–155.
41. F. Wang, C. M. Fan, C. Zhang, J. Lin, A localized space-time method of fundamental solutions for diffusion and convection-diffusion problems, *Adv. Appl. Math. Mech.*, **12** (2020), 940–958.
42. W. Qu, C. M. Fan, X. Li, Analysis of an augmented moving least squares approximation and the associated localized method of fundamental solutions, *Comput. Math. Appl.*, **80** (2020), 13–30.
43. W. Li, Localized method of fundamental solutions for 2D harmonic elastic wave problems, *Appl. Math. Lett.*, **112** (2021), 106759.
44. X. Li, S. Li, A linearized element-free Galerkin method for the complex Ginzburg–Landau equation, *Comput. Math. Appl.*, **90** (2021), 135–147.
45. X. Li, H. Dong, An element-free Galerkin method for the obstacle problem, *Appl. Math. Lett.*, **112** (2021), 106724.
46. X. Li, S. Li, A fast element-free Galerkin method for the fractional diffusion-wave equation, *Appl. Math. Lett.*, **122** (2021), 107529.
47. F. Wang, C. Wang, Z. Chen, Local knot method for 2D and 3D convection-diffusion-reaction equations in arbitrary domains, *Appl. Math. Lett.*, **105** (2020), 106308.
48. X. Yue, F. Wang, P. W. Li, C. M. Fan, Local non-singular knot method for large-scale computation of acoustic problems in complicated geometries, *Comput. Math. Appl.*, **84** (2021), 128–143.
49. W. Chen, M. Tanaka, A meshless, integration-free, and boundary-only RBF technique, *Comput. Math. Appl.*, **43** (2002), 379–391.
50. J. Sladek, V. Sladek, Y. C. Hon, Inverse heat conduction problems by meshless local Petrov–Galerkin method, *Eng. Anal. Bound. Elem.*, **30** (2006), 650–661.

AIMS Press